Preprint Cambridge Centre for Computational Chemical Engineering ISSN 1473 – 4273

A multi-compartment population balance model for high shear granulation

Kok Foong Lee[1], Sebastian Mosbach[1], Markus Kraft[1,2], Wolfgang Wagner[3]

released: 17 November 2014

[1] Department of Chemical Engineering
and Biotechnology
University of Cambridge
New Museums Site
Pembroke Street
Cambridge, CB2 3RA
United Kingdom
E-mail: mk306@cam.ac.uk

[2] School of Chemical
and Biomedical Engineering
Nanyang Technological University
62 Nanyang Drive
Singapore, 637459

[3] Weierstrass Institute for
Applied Analysis and Stochastics
Mohrenstraße 39
10117 Berlin
Germany
Email: wagner@wias-berlin.de

Preprint No. 149

Keywords: granulation, stochastic weighted algorithm, compartmental model, breakage, coalescence

Edited by
Computational Modelling Group
Department of Chemical Engineering and Biotechnology
University of Cambridge
New Museums Site
Pembroke Street
Cambridge CB2 3RA
United Kingdom

Fax: + 44 (0)1223 334796
E-Mail: c4e@cam.ac.uk
World Wide Web: http://como.cheng.cam.ac.uk/

Highlights

- A batch granulation process is modelled using a compartmental model.
- A population balance model for granulation is extended to have multiple compartments.
- A stochastic weighted algorithm is adapted to the population balance model.
- The compartmental model is optimised using experimentally measured size distribution.
- The fit to experimental data is improved with the compartmental model.

Abstract

This work extends the granulation model published by Braumann et al. (2007) (Chemical Engineering Science, 62, 4717-4728) to include multiple compartments in order to account for mixture heterogeneity encountered in powder mixing processes. A stochastic weighted algorithm is adapted to solve the granulation model which includes simultaneous coalescence and breakage. Then, a new numerical method to solve stochastic reactor networks is devised. The numerical behaviour of the new stochastic weighted algorithm is compared against the existing direct simulation algorithm. Lastly, the performance of the new compartmental model is then investigated by comparing the predicted particle size distribution against an experimentally measured size distribution. It is found that the new stochastic weighted algorithm exhibits superior performance compared to the direct simulation algorithm and the multi-compartment model produces results with better agreement with the experimental results compared to the original single-compartment model.

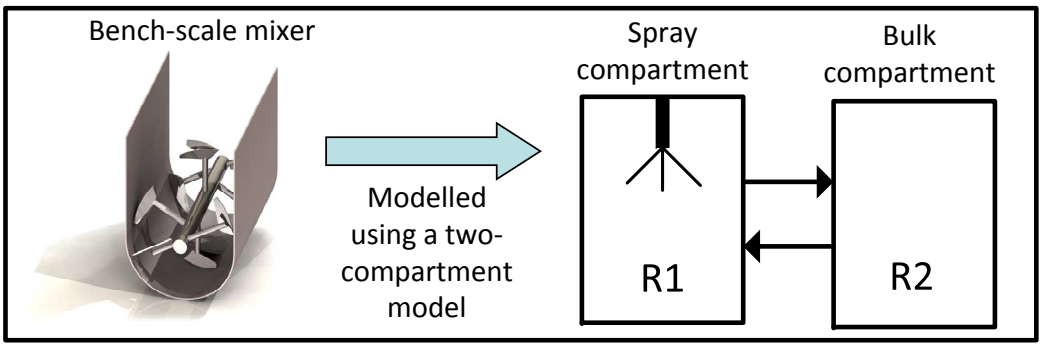

Contents

1 Introduction

Granulation is a size enlargement process to produce granules with desired properties. It is one of the key processes in the manufacture of fertilisers, detergents and pharmaceuticals. It is usually performed to reduce dustiness, which leads to improvements in powder handling and transportation.

Modelling approaches for wet granulation processes can be separated into two categories: population balance modelling and the discrete element method (DEM). The population balance approach tracks the change in the particle population with time through birth and death processes. For applications in granulation, these processes are usually the coalescence and breakage of particles [3]. On the other hand, in DEM, the motion of each particle and droplet is computed simultaneously using Newtonian equations of motion [6]. However, by itself, DEM does not consider the aggregation of granules and other processes [1], and it is also usually very computationally expensive.

The current work involves modelling a high shear granulation process using a population balance model through a stochastic modelling framework. Stochastic particle methods are able to simulate a high number of independent particle properties, in the case of granulation, the properties included in the modelling framework are usually solid content, liquid content, as well as porosity [1, 8, 9, 16, 23, 26].

Currently, there are two popular stochastic particle methods available in the literature: the direct simulation algorithm (DSA) and stochastic weighted algorithms (SWAs). In basic implementations of the DSA involving coagulation, the particle ensemble may be depleted to the point that there is only one computational particle left in the ensemble and this is avoided by duplicating the ensemble when the particle count falls below 50% [5]. Even then, it is often pointed out that the DSA produces unstable estimates of the concentrations of the rarer particles [21, 25]. Weighted particle methods, or SWAs may be used to counter these problems. In SWAs, each particle is given a statistical weight which is proportional to the number of particles represented by the computational particle. Instead of depleting the particle ensemble, coagulation events in SWAs adjust the statistical weights [25].

These stochastic particle methods are traditionally used to model processes without particle transport, implying that the system is perfectly mixed [5, 20]. However, in powder mixing process such as high shear granulation, advective or diffusive particle transport should not be ignored. Granulation processes usually proceed in three stages [15]: wetting and nucleation, consolidation and growth, and attrition and breakage. The nucleation stage is the process of bringing the liquid binder into contact with the powder and is often regarded as a very important stage in granulation processes [12]. In the mixer used in this work, not all powder particles are wetted in the same way and the assumption of uniformity breaks down. It is clear this has to be included in the model.

To account for the heterogeneous behaviour of powder mixing processes, several compartmental models have been proposed and these models often involve DEM simulations to gain particle flow data as input to the population balance models [2, 13, 18, 28]. However, not much attention is paid in implementing stochastic methods in compartmental models with particle transport. In most of the models, the transport of particles is included as an extra term in the population balance equations [10, 18, 19]. Just recently,

Menz et al. [22] presented a sequential modular approach to solve a reactor network with a multi-dimensional population balance model coupled to gas-phase chemistry using the stochastic approach. Irizarry [14] presented the 'particle bundle flow' method which ensures that particles will not hop across two domains in a single time step. In granulation, the stochastic approach is used by Bouffard et al. [2] to incorporate particle flow into their two-dimensional population balance model.

The main purpose of this paper is to include spatial inhomogeneity into an existing granulation model [3] with multiple compartments. In conjunction with this, a stochastic weighted algorithm [25] which improves numerical stability is adapted to this model. This paper also presents a new method to transport computational particles across different compartments.

This paper is structured as follows. In Sections 2 and 3, the population balance model and compartmental model are described in detail. Section 4 presents the algorithms used to solve the compartmental model, which include an adapted stochastic weighted algorithm that is crucial in providing numerical stability. Sections 5 and 6 assess the numerical issues and convergence in the stochastic particle methods. Lastly, the performance of the new compartmental model to reproduce experimental results is shown in Section 7.

2 Population balance model

2.1 Type-space

The type-space is the mathematical description of a particle. Here, the particle vector $x = (s_\mathrm{o},\, s_\mathrm{r},\, l_\mathrm{e},\, l_\mathrm{i},\, p)$ has five independent non-negative variables which describe a granule. They are original solid volume s_o, reacted solid volume s_r, external liquid volume l_e, internal liquid volume l_i, and pore volume p.

The following derived properties are defined in terms of the internal variables:

- **Particle volume**: The volume is calculated as:

$$v(x) = s_\mathrm{o} + s_\mathrm{r} + l_\mathrm{e} + p. \tag{1}$$

- **Mass**: Assuming that the densities of the liquids and the reacted solids are the same:

$$\rho_{l_\mathrm{e}} = \rho_{l_\mathrm{i}} = \rho_{s_\mathrm{r}}, \tag{2}$$

  the particle mass is calculated as:

$$m(x) = \rho_{s_\mathrm{o}} s_\mathrm{o} + \rho_{l_\mathrm{e}}(s_\mathrm{r} + l_\mathrm{i} + l_\mathrm{e}), \tag{3}$$

  where ρ_{s_o} and ρ_{l_e} are input parameters.

- **Porosity**:

$$\varepsilon(x) = \frac{p}{v(x)}. \tag{4}$$

2.2 Particle processes

Here, only the manner in which the processes are executed and their associated rates are covered, details such as the transformation rules for the jump processes are excluded. For the full description of the model and the reasoning behind the submodels, readers can refer to [3–5]. The processes are either implemented as jump processes or continuous processes. The jump processes include liquid addition, collision, and breakage, whereas the continuous processes include chemical reaction and penetration.

Liquid addition

Liquid droplets are introduced into the particle ensemble in the form of:

$$x = (0, 0, l_{\mathrm{e}}, 0, 0).$$

Two characteristic properties are needed to describe this process:

- $\dot{V}_{\mathrm{l}}$, the volumetric flow rate of the binder, and
- the droplet size distribution.

In the present work, we do not investigate the effects of droplet size distribution on the system and restrict all droplets to have the same size/type:

$$x = (0, 0, V_{\mathrm{droplet,mono}}, 0, 0).$$

Given that the volume of the droplets is $V_{\mathrm{droplet,mono}}$, the total number inflow rate is:

$$R_{\mathrm{droplet}} = \frac{\dot{V}_{\mathrm{l}}}{V_{\mathrm{droplet,mono}}}. \tag{5}$$

Collision

The rate of collision between two particles x_i and x_j is given by the kernel:

$$K(x_i, x_j) = n_{\mathrm{impeller}}\, k_{\mathrm{col}}, \tag{6}$$

where n_{impeller} (impeller speed) and k_{col} (rate constant) are input parameters. Collision events will lead to **coalescence** (the sticking of two particles together) and **compaction** of particles (reduction of pore volume). The occurrence of a successful coalescence event is governed by the Stokes criterion [11] and particles will undergo compaction regardless of the success of coalescence.

The Stokes criterion will yield the following outcomes in a collision event:

- *Successful coalescence*: The colliding particles coalesce. Provided that no droplets are involved, the resulting particle is also compacted:

$$x_i, x_j \mapsto T(x_i, x_j),$$

where

$$T(x_i, x_j) = \begin{cases} T_+(x_i, x_j) & \text{, if } x_i \text{ or } x_j \text{ is a droplet,} \\ \widehat{T}[T_+(x_i, x_j)] & \text{, otherwise.} \end{cases}$$

- *Unsuccessful coalescence*: The particles do not coalesce, but are compacted:

$$x_i, x_j \mapsto \widehat{T}(x_i), \widehat{T}(x_j).$$

T_+ represents the coalescence transformation rules and $\widehat{T}$ represents the compaction transformation rules [5]. The coalescence transformation creates a new particle by summing the contents of the colliding particles and calculates the pore volume of the new particle at the same time, whereas the compaction transformation reduces the pore volume at a rate proportional to the compaction rate constant k_{comp} (an input parameter).

Breakage

Based on [5], the breakage frequency of a parent particle x takes the form:

$$g(x) = \begin{cases} k_{\text{att}} U_{\text{imp}}^2 \left[\varepsilon(x) \Psi(x) + \dfrac{l_{\text{e}}}{v(x)} \right] v(x) & \text{, if } v(x) \geq v_{\text{parent,min}}, \\ 0 & \text{, otherwise,} \end{cases} \tag{7}$$

with input parameters k_{att} (attrition rate constant) and U_{imp} (impact velocity between the particles and the impeller blades) which depends on the impeller speed. $v_{\text{parent,min}}$ is the smallest parent particle that can be broken. The breakage frequency includes the function:

$$\Psi(x) = 1 - \min\left(\frac{s_{\text{r}}/(s_{\text{o}} + s_{\text{r}} + p)}{s_{\text{r}}^*}, 1 \right), \tag{8}$$

with the input parameter s_{r}^* (dimensionless critical amount of reacted solid so that the particle core does not break).

In the current model, the breakage transformation T_{B} on a particle x yields an 'abraded parent particle' x_i and a 'daughter particle' x_j:

$$T_{\text{B}}(x) \rightarrow x_i, x_j. \tag{9}$$

The particles x_i and x_j are restricted to have equal compositions (e.g. concentration of liquid), whereas their sizes are determined by a beta distribution.

Continuous processes within a particle

This model has two continuous processes within a particle, which are chemical reaction and penetration.

Chemical reaction refers to the solidification of binder, i.e. transformation of the liquid components (l_e and l_i) into reacted solid, s_r. The transformations of l_e and l_i into s_r occur at the rates $r_{reac,e}$ and $r_{reac,i}$ which are controlled by a rate constant k_{reac} [5].

Penetration refers to the diffusion of external liquid into the pores, i.e. transformation of l_e into l_i and occurs at the rate r_{pen} which is controlled by a rate constant k_{pen} [5].

Between jump events, the particles are modified according to the system of ordinary differential equations given below:

$$\frac{ds_o}{dt} = 0\,, \qquad \frac{ds_r}{dt} = r_{reac,e}(x) + r_{reac,i}(x)\,,$$

$$\frac{dl_e}{dt} = -r_{reac,e}(x) - r_{pen}(x)\,, \qquad \frac{dl_i}{dt} = -r_{reac,i}(x) + r_{pen}(x)\,, \qquad \frac{dp}{dt} = -r_{reac,i}(x)\,.$$

3 Compartmental model

Here, a batch granulation process is modelled as a series of well-mixed continuous-stirred tank reactors (CSTRs) to account for spatial inhomogeneity. A similar approach to perform particle transport developed by Menz et al. [22] is used in this work where each reactor in the network is given a characteristic residence time, τ.

In this study, two approaches to solve stochastic reactor networks are studied. The first approach is the direct approach which solves the whole network simultaneously and the second approach is the sequential modular approach used by Menz et al. [22]. Previously in the model considered by Menz et al. [22], the sequential approach is necessary due to the coupling between particle processes and gas phase reactions. In this work, the absence of gas phase reactions allows the network to be solved simultaneously.

The spreading of liquid binder in the powder bed is often regarded as a crucial stage in granulation processes [12, 15]. In order to capture the spreading of binder liquid in compartmental models, several groups of researchers [2, 13] include a spray compartment in their compartmental models. The network configuration used in this work is shown in Figure 1. The network is separated into two compartments: the spray compartment where liquid addition occurs and the bulk compartment. For the moment, we restrict the compartments to have equal volumes. Although we are only considering two compartments, this model can be easily extended to a n-compartment network.

4 Numerical method

This work investigates two popular stochastic particle methods to solve population balance models: the direct simulation algorithm (DSA) and a stochastic weighted algorithm

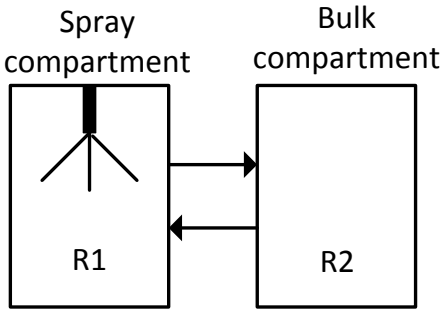

Figure 1: *Setup used in this study.*

(SWA).

The implementation of the DSA for this granulation model is described fully in [5]. Of particular interest in this work is the adaptation of a SWA [25] for this model which includes simultaneous breakage and coalescence.

Stochastic methods approximate the real system with a set of computational particles, where each computational particle represents a certain number of real particles [7, 22]. In this SWA, a statistical weight w is attached to each computational particle which is proportional to the number of particles represented by the computational particles [25].

4.1 Development of a stochastic weighted algorithm

Each compartment is described by a list of particles with statistical weights:

$$z(t)^{[k]} = \left((x_i, w_i), \quad i = 1, \ldots, n(t)^{[k]} \right) \qquad t \geq 0, \tag{10}$$

where $n(t)^{[k]}$ is the number of computational particles in compartment $[k]$ at time t and $[k]$ can be either R1 or R2. Each compartment is scaled by a normalisation parameter $V_N^{[k]}$ [5] that can be considered to represent a sample volume.

Liquid addition

In this SWA, liquid droplets are incepted with statistical weight $w = 1$. The jump rate for the inception of liquid droplets is (cf. (5)):

$$R_{\text{incep}}{}^{[k]} = \begin{cases} 2 \times \dfrac{\dot{V}_\text{l}}{V_{\text{droplet,mono}}} \dfrac{V_N^{[k]}}{V_{\text{reactor}}} & \text{, in the spray compartment,} \\ 0 & \text{, in the bulk compartment,} \end{cases} \tag{11}$$

where V_{reactor} is the volume of the reactor being modelled. The rate is doubled in the spray compartment because no liquid addition is performed in the bulk compartment. The term $V_N^{[k]}/V_{\text{reactor}}$ scales the rate according to the normalisation parameter.

Collision

Unlike in the DSA where collisions are symmetric, collision events are asymmetric in this SWA. Here, a pair of particles (x_i, w_i) and (x_j, w_j) collide at the rate of $K(x_i, x_j)w_j$.

The total jump rate for collisions in a compartment is [21]:

$$R_{\text{col}}{}^{[k]} = \frac{\sum_{i\neq j}^{n} K(x_i, x_j)w_j}{V_N^{[k]}}. \tag{12}$$

A collision event in this SWA has the following outcomes:

- *Successful coalescence*:

$$(x_i, w_i), (x_j, w_j) \mapsto \Big(T(x_i, x_j), \gamma(x_i, w_i, x_j, w_j)\Big), (x_j, w_j), \tag{13}$$

  where γ is the weight transfer function which defines how the statistical weights are manipulated. One of the well-behaved weight transfer functions from [25] is chosen to be used in this numerical study:

$$\gamma(x_i, w_i, x_j, w_j) = w_i \frac{m_i}{m_i + m_j}. \tag{14}$$

- *Unsuccessful coalescence*:

$$(x_i, w_i), (x_j, w_j) \mapsto (\widehat{T}(x_i), w_i), (\widehat{T}(x_j), w_j). \tag{15}$$

Since the number of computational particles remains constant, a variance reduction such as particle doubling is not required after coalescence events unlike in the DSA [5].

Breakage

The breakage frequency is unaffected by the weight and remains the same as Equation (7). The total jump rate for breakage in a compartment is given by:

$$R_{\text{break}}{}^{[k]} = \sum_{i=1}^{n} g(x_i). \tag{16}$$

The index i of the parent particle to break is chosen with the probability $g(x_i)/R_{\text{break}}{}^{[k]}$. During a breakage event, the parent particle is deleted and two new particles, x_i and x_j, are created. The new particles are given the same weight as the parent particle:

$$(T_B(x), w) \to (x_i, w), (x_j, w). \tag{17}$$

When the particle ensemble is full, random reduction [5] is employed to accommodate the new particles from breakage where a uniformly selected particle is removed.

Continuous processes within a particle

Processes within a particle that do not change the number of particles in the ensemble are performed in a similar way as in the DSA. Hence, the particles are modified according to the system of ordinary differential equations described in Section 2.2. The Linear Process Deferment Algorithm [24] is employed to accelerate the simulations, where these processes within a particle are the deferred processes.

4.2 Compartmental model: direct approach

The rate of particle outflow from a compartment $[k]$ is given by:

$$R_{\text{out}}{}^{[k]} = \frac{n(t)^{[k]}}{\tau^{[k]}}. \tag{18}$$

The outflow processes from the compartments are included as conventional jump processes [5] in addition to liquid addition, collision and breakage. Since there are two compartments, there are eight jump processes in total for this network.

Upon the selection of an outflow process in compartment $[k]$, a particle of index q is uniformly selected from compartment $[k]$ to be transferred to compartment $[l]$. Since only two compartments are involved, the selection of compartment $[l]$ is straightforward, i.e. if $[k]$ is R1, then $[l]$ is R2. In the DSA, it is represented by the jumps:

$$\begin{aligned} (x_q)^{[k]} &\rightarrow (x_r)^{[l]},\ (x_{r+1})^{[l]},\ \ldots,\ (x_{r+n_\text{c}-1})^{[l]}, \\ (x_q)^{[k]} &\rightarrow \text{ deleted}, \end{aligned} \tag{19}$$

where x_r is a copy of x_q from compartment $[k]$ and n_c is the number of copies made in compartment $[l]$. Note that particle x_q is deleted from compartment $[k]$ at the same time.

The number of copies to make is determined by the ratio of the normalisation parameters:

$$n_\text{c} = \begin{cases} \lfloor F_\text{c} \rfloor + 1 & \text{for } u < F_\text{c} - \lfloor F_\text{c} \rfloor \\ \lfloor F_\text{c} \rfloor & \text{otherwise,} \end{cases} \tag{20}$$

where

$$F_\text{c} = \frac{V_N^{[l]}}{V_N^{[k]}}, \tag{21}$$

and u is a pseudorandomly chosen real number such that $u \in [0,1]$.

As for the SWA here, the equivalent process is represented by the jumps:

$$\begin{aligned} (x_q, w_q)^{[k]} &\rightarrow (x_r, w_q \times F_\text{c})^{[l]}, \\ (x_q, w_q)^{[k]} &\rightarrow \text{ deleted}, \end{aligned} \tag{22}$$

Note that the statistical weight of the copied particle is adjusted instead of making multiple copies of it. The presence of statistical weights allows the number of transferred particles to be controlled more accurately than in the DSA.

4.3 Compartmental model: sequential modular approach

In contrast to the direct approach, the compartments are solved separately and the algorithm is shown in Figure 2. While a compartment is solved and steps forward in time, the other compartment is unaffected. In this case, an outflow process in a compartment does not contribute to an inflow process in the outlet compartment. So, a separate jump process for inflow is included in each compartment. Therefore, each compartment has five jump processes (liquid addition, collision, breakage, outflow and inflow).

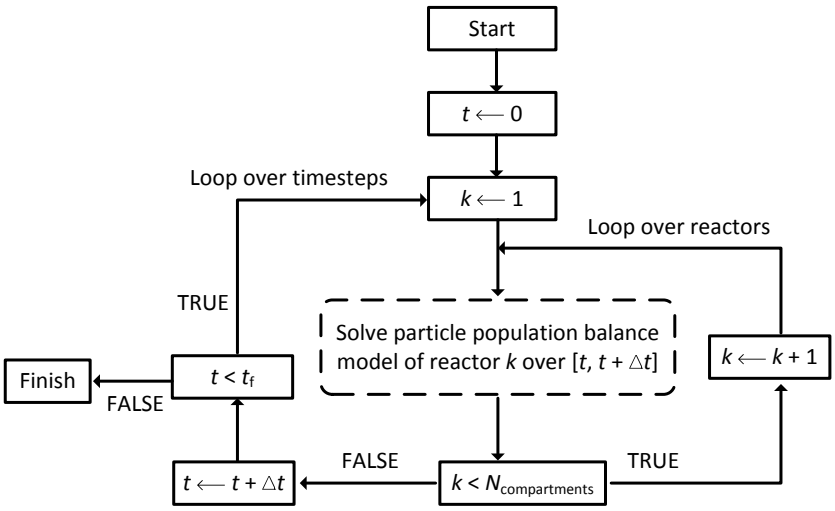

Figure 2: *Algorithm used to solve the reactor network with the sequential modular approach. Δt refers to the reactor time step and t_f refers to the simulation stop time.*

The jump rate for inflow in compartment $[k]$ is:

$$R_{\text{inflow}}{}^{[k]} = \frac{n(t)^{[l]}}{\tau^{[l]}}, \tag{23}$$

where $[l]$ refers to the inlet compartment. Since there are only two compartments, the selection of the inlet is simple, i.e. if $[k]$ is R1, then $[l]$ is R2.

Upon the selection of an inflow process in compartment $[k]$, a particle of index q is uniformly selected from compartment $[l]$ and copied into compartment $[k]$. In the DSA, it is represented by the jump:

$$(x_q)^{[l]} \rightarrow (x_r)^{[k]}, (x_{r+1})^{[k]}, \ldots, (x_{r+n_c-1})^{[k]} \tag{24}$$

where x_r is a copy of x_q from compartment $[l]$.

The value of n_c is determined by Equation (20), but the ratio of the normalisation parameters for this case is:

$$F_c = \frac{V_N^{[k]}}{V_N^{[l]}}. \tag{25}$$

On the other hand, an inflow process for the SWA here is represented by the jump:

$$(x_q, w_q)^{[l]} \rightarrow (x_r, w_q \times F_c)^{[k]}. \tag{26}$$

Note that in both cases, the particle x_q from compartment $[l]$ is simply copied and not deleted from its source.

The rate of particle outflow remains the same as Equation (18) but is performed slightly differently. Upon the selection of an outflow process in compartment $[k]$, a uniformly selected particle is simply deleted:

$$(x_q)^{[k]} \rightarrow \text{deleted}. \tag{27}$$

5 Numerical studies

In this section, the numerical studies that investigate the effects of the stochastic algorithm parameters are presented. The investigated numerical parameters are the maximum number of computational particles in each compartment, $N_{\max}$, and the number of stochastic runs, L. In this work, $N_{\max}$ is set to be equal for both compartments.

For simulations with multiple runs, the temporal evolution of a functional $M(t)$ is averaged over the number of runs:

$$\eta_1^{(N_{\max},L)}(t) = \frac{1}{L}\sum_{l=1}^{L} M^{(N_{\max},l)}(t), \tag{28}$$

where a functional refers to a measured ensemble property such as total mass. Descriptions of the investigated functionals can be found in Section 5.3.

The empirical variance is:

$$\eta_2^{(N_{\max},L)}(t) = \frac{1}{L}\sum_{l=1}^{L} M^{(N_{\max},l)}(t)^2 - \eta_1^{(N_{\max},L)}(t)^2, \tag{29}$$

and the confidence intervals are constructed as:

$$\eta_1^{(N_{\max},L)}(t) \pm a_P \sqrt{\frac{\eta_2^{(N_{\max},L)}(t)}{L}}, \tag{30}$$

where P is the confidence level. In this work, we use $a_P = 1.64$, which corresponds to $P = 0.9$.

5.1 Simulation conditions

The experimental system considered in this work is the wet granulation of lactose powder using deionised water as the binder and its full description can be found in [17]. For the

simulations, a set of experimental conditions is chosen from [17, Experiment B1]. The experimental conditions are listed in Table 1 and described briefly here.

Each compartment is initialised with a set of non-porous particles of the form:

$$x = (s_o, 0, 0, 0, 0) \tag{31}$$

following the measured size distribution of the lactose powder ($\mu_{psd} = 38.93\ \mu$m, $\sigma_{psd} = 1.6\ \mu$m). With the exception of the results shown in Figure 5, the number of initialised particles in each compartment, $n(0)^{[R1]}$ and $n(0)^{[R2]}$, is set at $0.75\ N_{max}$. In the SWA here, the particles are initialised with statistical weight $w = 1$.

Once the solid particles are initialised, liquid droplets are added at the rate represented by Equation (11) and stopped after 120 seconds. The simulations are then allowed to continue for 300 seconds after the liquid addition phase and this refers to the wet massing time in Table 1.

The rate parameters used in the numerical studies are listed in Table 2. From a previous study involving this model [17], it was found that the collision rate is the most significant parameter which affects the results. Hence, it is also decided to focus on the collision rate in this numerical study by assigning different collision rate constants to both of the compartments while keeping the other rate constants equal. Lastly, it is assumed that the network operates at steady state by assigning equal residence times to both reactors.

5.2 Key numerical issue

The key numerical issue encountered during the implementation of the new compartmental model is caused by the different values of $V_N^{[k]}$ in each compartment.

The initial values of $V_N^{[k]}$ are determined by the values of $n(0)^{[k]}$ [5]. Here, it is important to note that the number of particles in the compartments is purely a numerical parameter and should not affect the results provided the solution has converged (when the number of particles is sufficiently large). Since each compartment is initialised with an equal number of particles in this study, the initial values of $V_N^{[k]}$ are equal. However, the values of $V_N^{[k]}$ change by particle doubling and random reduction, which are done to keep the number of particles within the prescribed region [5]. These processes cause the values of $V_N^{[k]}$ to be different in each compartment and caused numerical instability especially in the DSA, which is highlighted in Section 6.1.

5.3 Functionals

In this work, a functional refers to a calculated overall property of the particle ensembles. The main purpose of using a compartmental model for a batch process is to account for the heterogeneity in powder mixing. Hence, it is desired to derive overall properties from the simulations. From a physical perspective, the calculations of the functionals adopted here are analogous to taking samples with equal volumes from each compartment which are then lumped together for analysis.

Table 1: *Model physical parameters.*

Description	Symbol	Value
Known process settings		
Material density	ρ_{s_o}	1545.0 kg/m^3
Binder density	ρ_{l_e}	998.0 kg/m^3
Binder viscosity	η	1.0×10^{-3} Pa s
Impeller radius	-	72.5×10^{-3} m
Reactor volume	V_{reactor}	3.0×10^{-3} m^3
Impeller speed	n_{impeller}	2 rev/s
Binder flow rate	$\dot{V}_l$	1.25×10^{-6} m^3/s
Wet massing time	-	300 s
Binder to powder ratio	-	150 ml:1000 g
Model parameters – approximated		
Powder size distribution; location	μ_{psd}	38.93 μm
Powder size distribution; shape	σ_{psd}	1.6 μm
Droplet size distribution; location	μ_{dsd}	70.0 μm
Droplet size distribution; shape	σ_{dsd}	1.0 μm
Number of real particles	-	6.5×10^9
Solid coefficient of resistance	e_{s_o}	1.0
Reacted coefficient of resistance	e_{s_r}	1.0
Liquid coefficient of resistance	e_{l_i}	1.0
Asperities height	H_a	2.09×10^{-7} m
Particle-particle collision velocity	U_{col}	9.11×10^{-2} m/s
Minimum particle porosity after compaction	-	0.25
Breakage; maximum fraction of the particle that can break	ν_{max}	5.0
Breakage; proportion	$\nu_{\text{min,max}}$	1.1
Breakage; minimum fragment volume	$v_{\text{frag,min}}$	5.236×10^{-13} m^3
Breakage; distribution	α_{daughter}	5.0
Breakage; distribution	β_{daughter}	2.0
Breakage; critical reacted solid	s_r^*	1.0×10^{20}
Breakage; particle-impeller impact velocity	U_{imp}	0.82 m/s

As each compartment is scaled by a unique normalisation parameter $V_N^{[k]}$, the difference has to be taken into account while calculating the functionals. This is because whilst the actual sizes of the compartments are equal, they are represented by ensembles with different sample volumes. For a compartment with smaller V_N, each computational particle represents a higher number of real particles compared to a computational particle in a compartment with larger V_N. Therefore, the particle ensembles have to be scaled accordingly before making any calculations. In the current implementation, the value of $V_N^{[\text{R2}]}$ is scaled to the value of $V_N^{[\text{R1}]}$.

In the DSA, each particle in R1 is given a statistical weight $w = 1$. In R2, each particle is

Table 2: *Rate parameters for the numerical studies.*

Parameter	Value		Unit
	R1	R2	
k_{col}	1.00×10^{-12}	1.00×10^{-14}	m^3
k_{comp}	1.07×10^{-14}	1.07×10^{-14}	s/m
k_{att}	1.00×10^{7}	1.00×10^{7}	s/m^5
k_{pen}	28.0	28.0	$\text{kg}^{1/2}\text{m}^{7/2}/\text{s}^{3/2}$
k_{reac}	6.19×10^{-13}	6.19×10^{-13}	m/s
τ	200	200	s

given a statistical weight of:

$$w = V_N^{[\text{R1}]}/V_N^{[\text{R2}]}. \tag{32}$$

A similar scaling approach is adopted for the SWA here. Particle weights in R1 are left unchanged. In R2, the weights are modified according to:

$$w_{\text{new}} = w_{\text{old}} \times V_N^{[\text{R1}]}/V_N^{[\text{R2}]}. \tag{33}$$

After scaling the ensembles, the total value of V_N for the entire network is calculated as:

$$\sum V_N = V_N^{[\text{R1}]} \times 2. \tag{34}$$

By taking into account the modified statistical weights, the functionals are calculated according to the formulae listed in Table 3.

6 Results

In the following sections, the compartmental model is solved using the direct approach, with the exception of the results in Section 6.3.

6.1 Error in transport

Before attempting to gain any useful information from the compartmental model, it is important to ascertain that the transport of particles is performed in a manner which conserves mass. Looking at Equations (19 - 22) and (24 - 26), it is inevitable that the transport of particles will cause some error in the system, especially in the DSA where the number of copies is determined randomly.

Table 3: *Functionals for the compartmental model.*

$M(t)$	Description	Formula	Units
$M_0(t)$	Particle number concentration	$\frac{1}{\sum V_N}\sum w_i$	m^{-3}
$M_1(t)$	First volume moment	$\frac{1}{\sum V_N}\sum w_i\, v(x_i)$	[-]
$M_2(t)$	Second volume moment	$\frac{1}{\sum V_N}\sum w_i\, v(x_i)^2$	m^3
$\mu_{\mathrm{psd}}(t)$	Particle geometric number mean size	$\exp\left(\frac{\sum w_i \ln d(x_i)}{\sum w_i}\right)$	m
$\sigma_{\mathrm{psd}}(t)$	Particle geometric number standard deviation	$\exp\sqrt{\frac{\sum w_i(\ln(d(x_i)/\mu_{\mathrm{psd}}))^2}{\sum w_i}}$	[-]
$\overline{\varepsilon}(t)$	Number averaged porosity	$\frac{1}{\sum w_i}\sum w_i\, \varepsilon(x_i)$	[-]
$m_{\mathrm{total}}(t)$	Normalised total mass	$\frac{\sum w_i\, m(x_i)}{\sum V_N}$	$\mathrm{kg\ m}^{-3}$

The normalised total mass of the network, m_{total}, defined in Table 3 is used as the key quantity of this study. As a reference, a test run is performed by only adding liquid droplets into the system without simulating any other processes.

Figures 3 and 4 show the comparison of total mass between the liquid addition only simulations and the simulations performed with the rate parameters in Table 2.

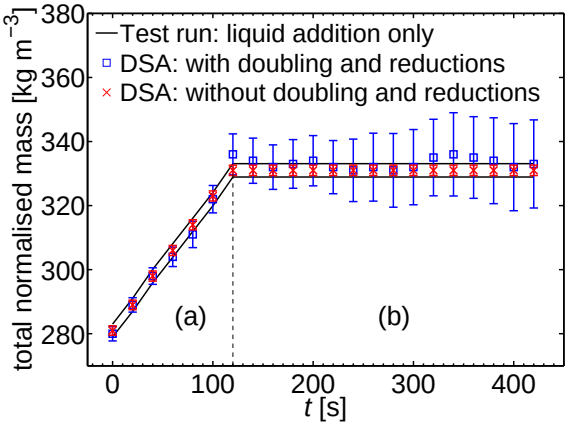

Figure 3: *Total normalised mass for the DSA ($N_{\mathrm{max}} = 16384$, $L = 16$). The two lines for the test run show the upper- and lower-bound of the confidence interval. Particle transport is performed using the direct approach. (a) Liquid addition phase. (b) Wet massing phase.*

Figure 3 presents the total mass in the network for the DSA. The first set of data (represented by the blue squares) is obtained by running the model in the conventional way with the doubling algorithm and random reduction enabled whereas the second set of data (represented by the red crosses) is obtained by running the model with the doubling algorithm disabled. It is evident that with the doubling algorithm enabled, the total mass in the system fluctuates. In this case, the normalisation parameters of the compartments vary with time through ensemble doubling and random reductions. As such, the value of F_c is usually not an integer. This makes it difficult to transfer the accurate amount of particles across the network because the number of copies to make in a transfer event is determined randomly in the DSA.

This deduction is confirmed by the second set of data with the doubling algorithm disabled. In the current setup, the rate of coalescence is sufficiently high compared to the rate of breakage, so there is no need for random reduction because the particle ensembles are never full. As both compartments are initialised with an equal number of particles and the initial value of $V_N^{[k]}$ is determined by the value of $n(0)^{[k]}$ [5], the value of F_c is held at 1.0 throughout the simulation. It can be observed that the errors from transport are greatly reduced when the value of F_c is held as an integer. This might suggest that it is favourable to run the DSA without the doubling algorithm, but it is shown later in Section 6.2 that the doubling algorithm is required to reduce the systematic error in the estimation of other functionals.

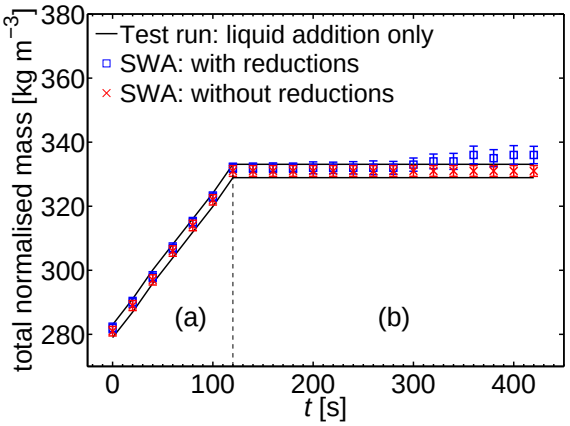

Figure 4: *Total normalised mass for the SWA ($N_{\max} = 16384$, $L = 16$). The two lines for the test run show the upper- and lower-bound of the confidence interval. Particle transport is performed using the direct approach. (a) Liquid addition phase. (b) Wet massing phase.*

On the other hand, Figure 4 shows that the SWA developed in this work produces results which are much more numerically stable compared to the DSA. The first set (represented by the blue squares) is obtained by running the model with the rates listed in Table 2. It can be observed that even though the mass content is much more stable compared to the DSA, there is a slight systematic error towards the end of the simulation. A very likely cause for this error is due to the random reductions performed when the particle ensemble is full to accommodate the new particles from breakage events.

The second set of results (represented by the red crosses) in Figure 4 is obtained by running a simulation without breakage ($k_{\text{att}} = 0$) while keeping the other rate constants at their original values. From this plot, it is clear that without random reductions, this SWA is able to maintain the mass content within the network accurately.

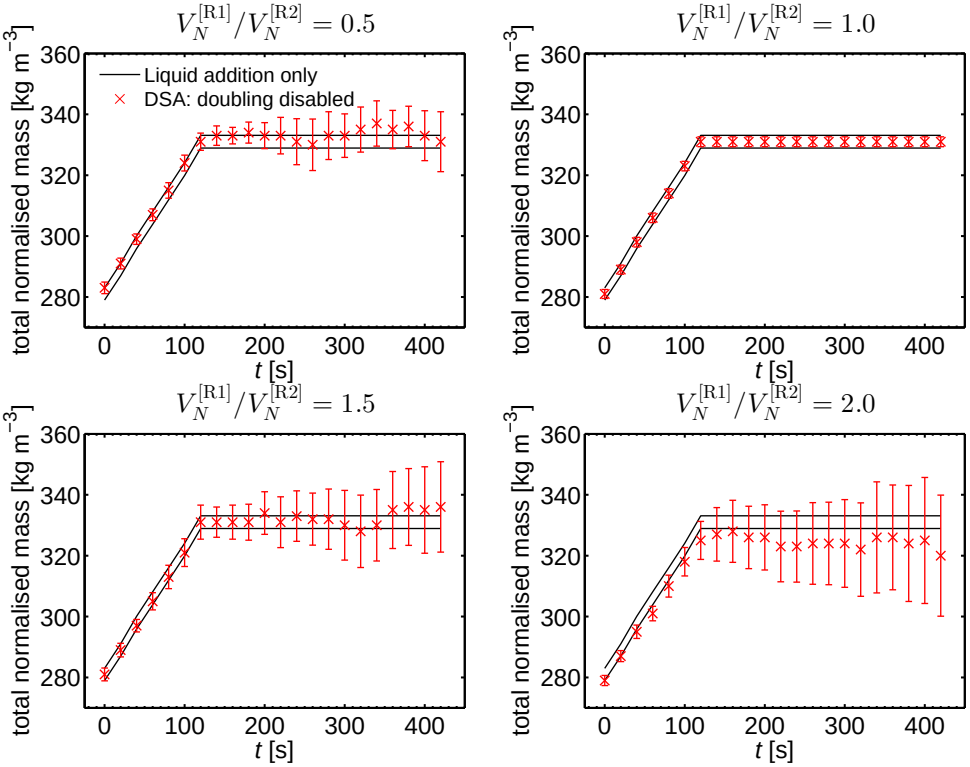

Figure 5: *Total normalised mass for different values of $V_N^{[R1]}/V_N^{[R2]}$. ($N_{\max} = 16384$, $L = 16$). The two lines for the test run show the upper- and lower-bound of the confidence interval. Particle transport is performed using the direct approach.*

As indicated in Figure 3, it is clear that the DSA will become numerically unstable when the normalisation parameters $V_N^{[k]}$ are different in each compartment. To prove this, Figure 5 shows the results from four separate simulations initialised with different values of $V_N^{[R1]}/V_N^{[R2]}$, thus giving different values of F_c. In these simulations, the doubling algorithm is disabled, therefore the values of F_c for each compartment are held constant. The respective values of $n(0)^{[k]}$ to set the values of $V_N^{[R1]}/V_N^{[R2]}$ are listed in Table 4. From this figure, we can confirm that the sole source of error in the DSA is from the transport of particles because the DSA can only maintain the accurate amount of mass in the system when the values of $V_N^{[k]}$ for both compartments are equal.

6.2 Convergence of functionals

Here, two sets of results are shown in Figures 6 and 7. They highlight the importance of the doubling algorithm to reduce systematic errors in the DSA and also the ability of the

Table 4: *Values of $V_N^{[\mathrm{R1}]}/V_N^{[\mathrm{R2}]}$ for the simulations presented in Figure 5.*

$V_N^{[\mathrm{R1}]}/V_N^{[\mathrm{R2}]}$	$n(0)^{[\mathrm{R1}]}$	$n(0)^{[\mathrm{R2}]}$
0.5	$0.375\,N_{\max}$	$0.750\,N_{\max}$
1.0	$0.750\,N_{\max}$	$0.750\,N_{\max}$
1.5	$0.750\,N_{\max}$	$0.500\,N_{\max}$
2.0	$0.750\,N_{\max}$	$0.375\,N_{\max}$

SWA developed here to approximate the functionals at much fewer stochastic particles. In these figures, the results are compared with a high-precision solution obtained by running the model with $N_{\max} = 262144$, $L = 10$ using this SWA. This convergence study is conducted by varying $N_{\max}$ and L while holding their product $N_{\max} \times L$ at 2^{18} to keep the computational times constant.

From these figures, it is clear that the doubling algorithm is required to reduce the systematic errors especially for the second moment, M_2, at lower particle numbers. Without the doubling algorithm, coalescence events will deplete the particle ensembles and increase the systematic errors. It is also clear from these figures that this SWA reaches convergence at a lower $N_{\max}$ compared to the DSA. At $N_{\max} = 512$ (Figure 6), this SWA is already producing results which are nearly identical to the high-precision solution. On the other hand, the DSA requires at least $N_{\max} = 2048$ (Figure 7) to produce reasonably accurate results.

6.3 Comparison between the direct approach and the sequential modular approach to transport particles

All the results shown thus far are simulated using the direct approach. Here, the performance of the sequential modular approach (with $\Delta t = 1$s) is compared with the direct approach and the results are shown in Figure 8. It is obvious that as long as Δt is small enough, the sequential modular approach will produce identical results with the direct approach. There is also negligible difference in computational times for both approaches. Hence, it is recommended to use the direct approach to simulate stochastic reactor networks unless it is necessary to use the sequential modular approach because there is one less numerical parameter, Δt, to be considered.

6.4 Computational efficiency

The computational time required to simulate the wet granulation test system as a function of $N_{\max}$ is investigated in this section. These calculations are performed on a desktop computer with a 3.30 GHz quad core Intel processor and 8 GB of RAM.

Figure 9 shows the CPU times per run of the DSA and SWA simulations for increasing $N_{\max}$. For a given value of $N_{\max}$, the CPU time for this SWA is typically about three times

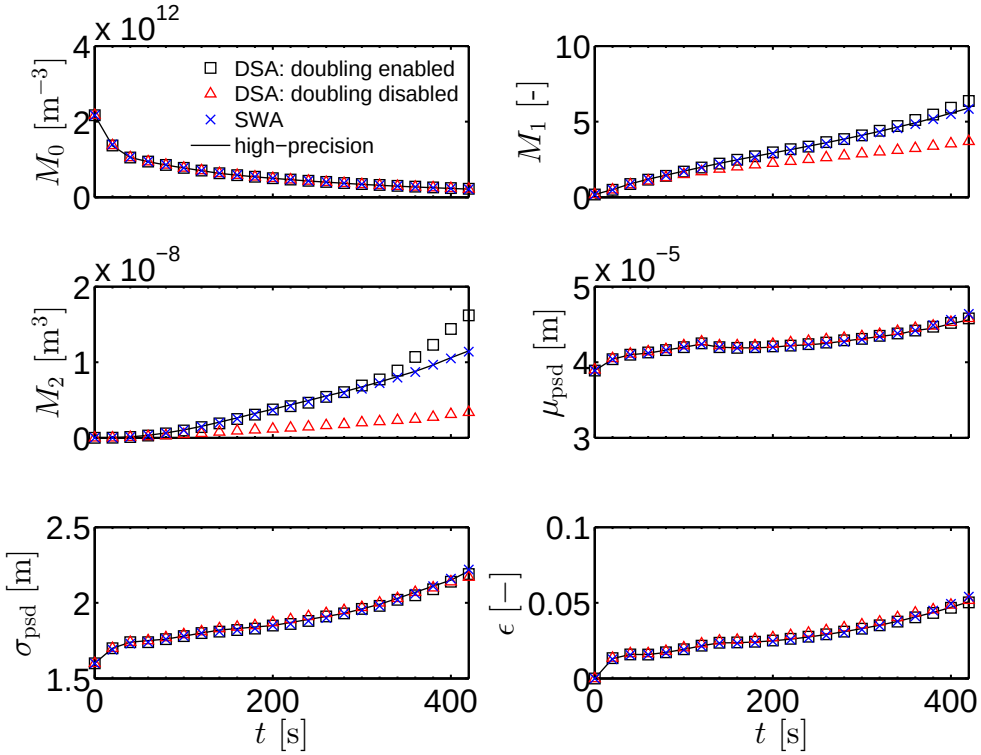

Figure 6: *Temporal evolution of the ensemble properties listed in Table 3 with* $N_{\max} = 512$, $L = 512$. *The confidence intervals are not shown because they are smaller than the size of the symbols. Particle transport is performed using the direct approach.*

more than the equivalent DSA simulation.

The additional CPU time required by this SWA is due to the increased number of simulated events, which is shown in Figure 10. As this SWA emphasises the calculations of the rare larger particles with low statistical weights [25], more coalescence events are required to capture a decrease in particle number concentration compared to the DSA. Consequentially, as the larger particles have higher breakage frequencies because they have higher pore volumes, the number of breakage events in this SWA is also significantly higher than the equivalent DSA simulation.

In order to compare the efficiency of the algorithms, the computational times per run for a given error for both algorithms are compared. For this, the total error for a given simulation is estimated by calculating the relative average absolute error $\bar{e}$ of the second moment M_2 over I time intervals:

$$\bar{e}_{M_2}(N_{\max}, L) = \frac{1}{I} \sum_{i=1}^{I} \frac{|\eta_{1,M_2}^{(N_{\max},L)}(t_i) - \zeta_{M_2}(t_i)|}{\zeta_{M_2}(t_i)}, \tag{35}$$

where ζ is the high-precision solution.

The calculated errors are shown in Figure 11. It is found that the DSA requires at least

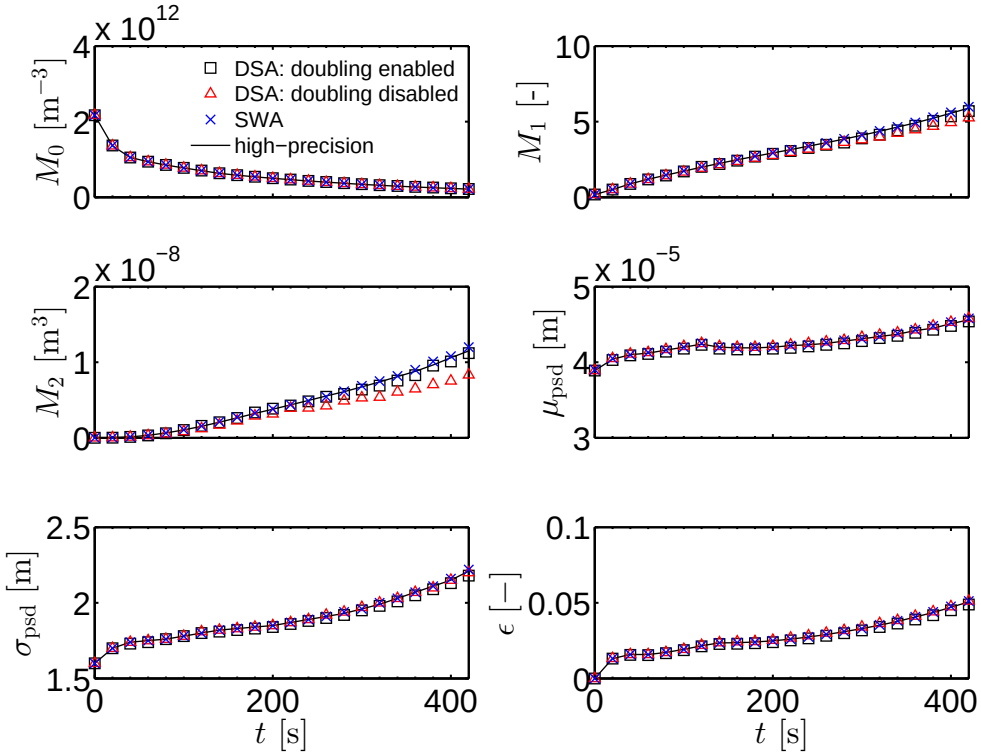

Figure 7: *Temporal evolution of the ensemble properties listed in Table 3 with* $N_{\max} = 2048$, $L = 128$. *The confidence intervals are not shown because they are smaller than the size of the symbols. Particle transport is performed using the direct approach.*

$N_{\max} = 2048$ to achieve a reasonably converged result compared to this SWA which requires only $N_{\max} = 256$ for the equivalent error. The CPU times per run for these simulations are 0.45s (DSA) and 0.15s (SWA) respectively. Therefore, this SWA is the more efficient algorithm as it requires less CPU time for a given error even though it requires more CPU time compared to the DSA for the equivalent $N_{\max}$.

7 Application

The performance of the new multi-compartment granulation model to reproduce experimental results is investigated in this section. From the numerical studies in the previous sections, it is evident that the SWA described in Section 4.1 is the preferred algorithm for simulating compartmental models, hence, the results in this section are obtained using this SWA.

The same experimental conditions listed in Table 1 are used for the study here. As such, the experimental data used here is also obtained from [17]. The best fit results are obtained by using the empirical cumulative size distribution as the criterion for optimisation.

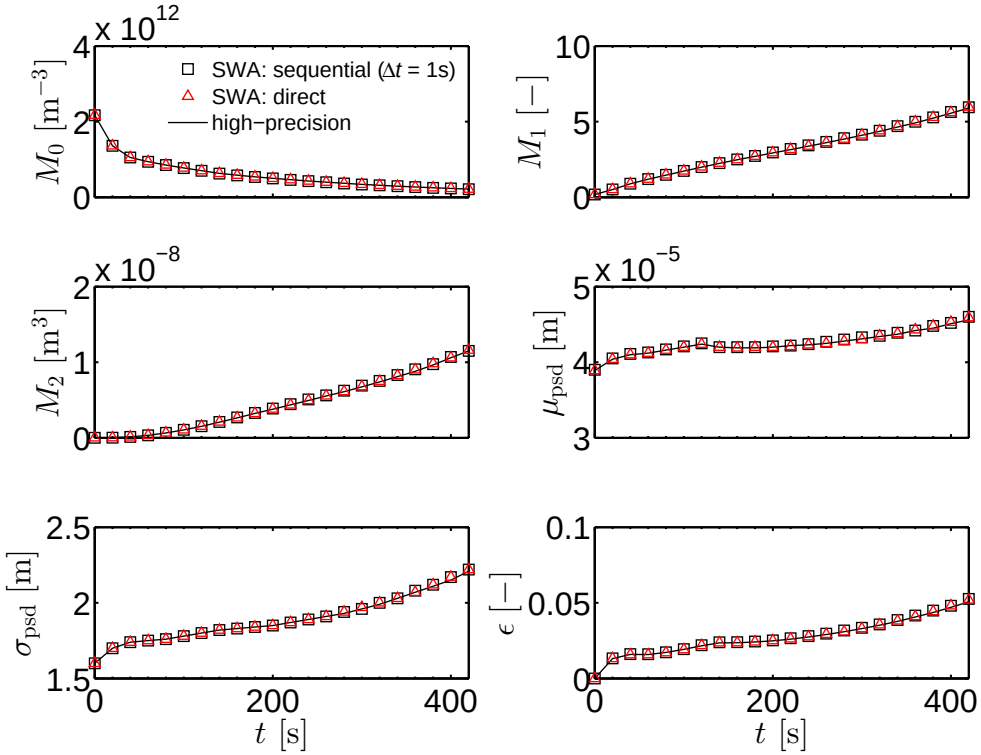

Figure 8: *Comparison between the direct approach and the sequential approach with* $N_{\max} = 16384$*,* $L = 16$*. The confidence intervals are not shown because they are smaller than the symbol size.*

The empirical cumulative distribution function Q_3, is calculated directly from the mass fractions as:

$$Q_{3,i} = \sum_{j=1}^{i} d_j, \text{ for } i = 1, \ldots, N_S, \tag{36}$$

where d_j is the mass fraction of the jth sieve class and N_S is the number of sieve classes.

A similar methodology to optimise the model presented by Kastner et al. [17] is adopted here. The process begins by defining the boundaries of the model parameter space. Then, Sobol sequences are used to sample the bounded parameter space. The model is then evaluated at the generated Sobol points. Finally, the best Sobol point is determined by the objective function defined below, which is the Euclidean distance:

$$OF = \sqrt{\sum_{i=1}^{Y} (y_i^{\text{sim}} - y_i^{\text{exp}})^2}, \tag{37}$$

where Y is the number of responses for the defined criterion (which is N_S for this case), y^{sim} is the response from the simulation and y^{exp} is the response from the experimental data.

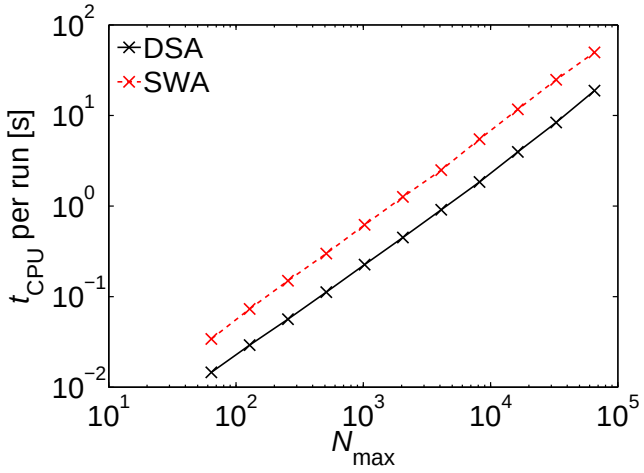

Figure 9: *Average CPU time required per run as a function of number of stochastic particles. Particle transport is performed using the direct approach.*

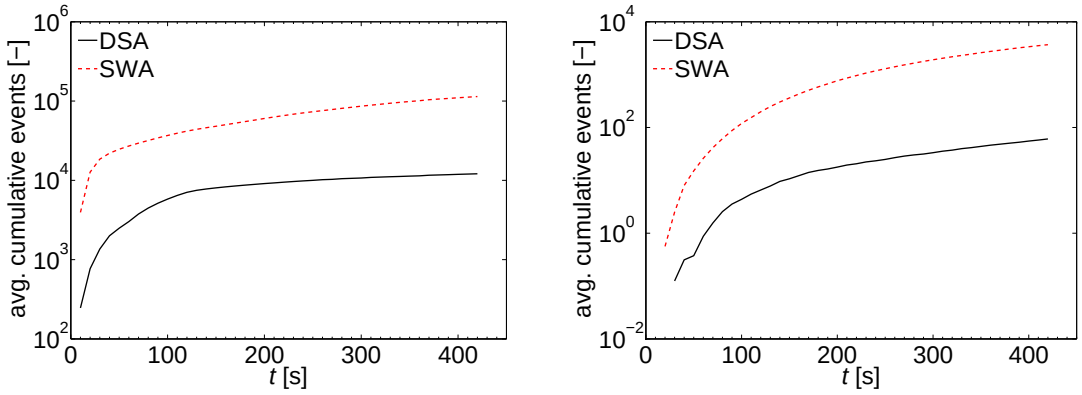

(a) *Coalescence* **(b)** *Breakage*

Figure 10: *Average cumulative number of events obtained with* $N_{\max} = 16384$, $L = 16$. *Particle transport is performed using the direct approach.*

In a preliminary sensitivity analysis, it was found that the influence of the collision rate constant over the generated size distribution is much greater than that of the other rate constants. Hence, to reduce the number of dimensions to consider in the parameter space, only the collision rate constant is allowed to be different between the compartments and the other rate constants are set to be equal across the network. The parameter space used in the simulations is presented in Table 5. The choice of ranges for the rate constants are similar to the study performed in [17], e.g. the collision rate needs to be sufficiently high in order to form the larger granules measured from experiments. As for the choice of the range for τ, the lower bound is chosen such that the rate of particle transfer is not so great that the system is perfectly mixed, and the upper bound is chosen such that there is observable difference when the model is simulated without any particle transport. To obtain the best sets of parameters, a total of 10000 simulations were performed within the parameter space for each network configuration.

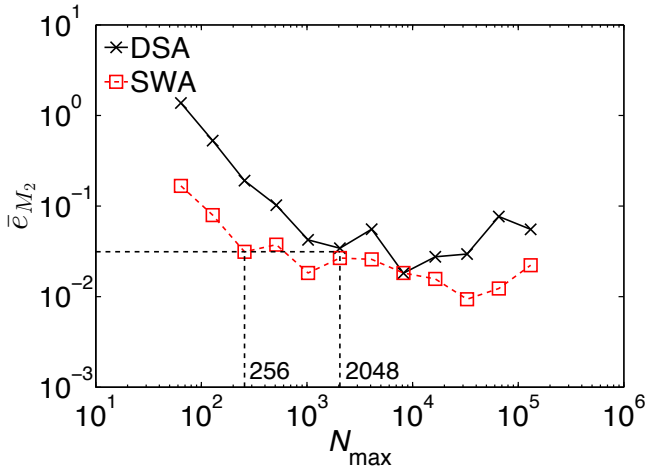

Figure 11: *Relative average absolute errors of M_2 plotted against N_{max}.*

Table 5: *Parameter space used in the simulations.*

Parameter	Lower bound	Upper bound	Scaling	
k_{col}	1×10^{-16}	1×10^{-11}	logarithmic	→ Different in each compartment
k_{comp}	1×10^{-15}	1×10^{-12}	logarithmic	} Equal in all compartments
k_{att}	1×10^{1}	1×10^{6}	logarithmic	
k_{pen}	1×10^{1}	1×10^{6}	logarithmic	
k_{reac}	5×10^{-16}	5×10^{-9}	logarithmic	
τ	60	1000	linear	

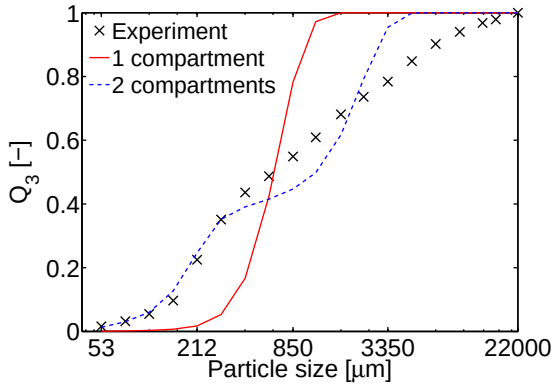

Figure 12: *Best fit empirical cumulative distributions. Simulations are performed with $N_{max} = 16384$ and $L = 16$. Particle transport is performed using the direct approach.*

Figure 12 shows the best fit empirical cumulative distributions obtained within the parameter space and the best estimated parameters are listed in Table 6. By accounting for the effects of heterogeneity in powder mixing processes, the model is now able to re-

produce wider size distributions which conforms to our experimental data. There is also experimental evidence that non-uniform binder distribution plays a significant role in determining the properties of the final product [27], supporting the use of compartmental models.

Table 6: *Best estimated parameters.*

Parameter	Number of compartments		
	1	2	
		R1	R2
k_{col}	1.09×10^{-13}	8.56×10^{-15}	1.82×10^{-12}
k_{comp}	5.27×10^{-15}	1.10×10^{-15}	1.10×10^{-15}
k_{att}	47108.10	23727.10	23727.10
k_{pen}	3629.23	115.67	115.67
k_{reac}	8.36×10^{-14}	1.26×10^{-09}	1.26×10^{-09}
τ	-	895.58	895.58
OF	0.81	0.32	

8 Conclusion

In this work, a SWA is adapted to a multi-dimensional granulation model which involves simultaneous coalescence and breakage. In addition to this, two approaches to solve stochastic reactor networks are also presented, which include a direct approach that considers all the processes in the network simultaneously and a sequential modular approach that solves the network in a stepwise fashion.

The error from transporting particles across the network was investigated in detail by examining the total mass in the system. It was found that this SWA is strongly favoured to minimise the stochastic noise due to transport. Next, the convergence of the calculated functionals was investigated as a function of the maximum number of computational particles. It was found that this SWA requires much fewer computational particles for a fixed error compared to the DSA. Besides that, it was also shown that this SWA requires less CPU time compared to the DSA to achieve an equivalent accuracy.

As a result from this work, it can be concluded that this SWA is the preferred algorithm to solve stochastic reactor networks due to the substantial numerical stability it provides. Hence, the compartmental model will be simulated using this SWA when it is used to predict experimental results in the future. Furthermore, it was shown that with just two compartments, the fit to a set of experimental data is dramatically improved.

The present work shows that SWAs can be used to solve complex population balance models with multiple processes which include particle transport, coalescence, and breakage. This is particularly suited for powder mixing processes where the assumption of perfect mixing is poor and particle flow heterogeneity should not be ignored.

As it was pointed out that there are systematic errors in mass for this SWA when there are significant breakage events, an immediate future work will involve the modification of the breakage algorithm for this SWA such that only one computational particle is changed at a time instead of introducing new particles into the system. On the other hand, using size distribution as the only physical quantity to optimise the model is insufficient. Therefore, another further step to make is to improve the characterisation of the product, which may include using experimentally measured porosities to optimise the model.

Acknowledgements

Useful discussions with Dr William Menz are gratefully acknowledged. This project is partly funded by the National Research Foundation (NRF), Prime Minister's Office, Singapore under its Campus for Research Excellence and Technological Enterprise (CREATE) programme. Support of the Weierstrass Institute for Applied Analysis and Stochastics (WIAS) in Berlin is also gratefully acknowledged.

Nomenclature

Roman symbols

a_P	constant for confidence intervals	[-]
d	mass fraction for an individual sieve class	[-]
e	particle coefficient of restitution	[-]
e_{coag}	coalescence coefficient of restitution	[-]
$e_{l_{\text{i}}}$	liquid coefficient of resistance	[-]
$e_{s_{\text{o}}}$	solid coefficient of resistance	[-]
$e_{s_{\text{r}}}$	reacted solid coefficient of resistance	[-]
F_{c}	ratio of normalisation parameters	[-]
g	breakage frequency	s^{-1}
H_{a}	height of asperities	m
K	coalescence kernel	$\text{m}^3\ \text{s}^{-1}$
k_{att}	attrition rate constant	$\text{s}\ \text{m}^{-5}$
k_{col}	collision rate constant	m^3
k_{comp}	compaction rate constant	$\text{s}\ \text{m}^{-1}$
k_{pen}	penetration rate constant	$\text{kg}^{0.5}\ \text{s}^{-1.5}\ \text{m}^{-3.5}$
k_{reac}	reaction rate constant	$\text{m}\ \text{s}^{-1}$
L	number of stochastic runs	[-]
l_{e}	external liquid volume	m^3
l_{i}	internal liquid volume	m^3
M	calculated ensemble property	[-]
M_0	Particle number concentration	m^{-3}
M_1	First volume moment	[-]
M_2	Second volume moment	m^3
m	mass of particle	kg
m_{total}	total normalised mass in the network	$\text{kg}\ \text{m}^{-3}$
N_{max}	maximum number of computational particles	[-]
N_{S}	number of sieve classes	[-]
$N_{\text{compartment}}$	number of compartments	[-]
n	number of computational particles	[-]
n_{c}	number of copies to make	[-]
n_{impeller}	impeller speed	$\text{rev}\ \text{s}^{-1}$
OF	objective function	[-]
P	confidence level	[-]
p	pore volume	m^3
Q_3	empirical cumulative distribution function	[-]
R	particle radius	m
R_{break}	rate of breakage	s^{-1}
R_{col}	rate of collisions	s^{-1}
R_{droplet}	number inflow rate of droplets	s^{-1}

R_{incep}	rate of inception	s^{-1}
R_{inflow}	rate of inflow	s^{-1}
R_{out}	rate of particle outflow	s^{-1}
r_{pen}	rate of penetration	$\text{m}^3\ \text{s}^{-1}$
$r_{\text{reac,e}}$, $r_{\text{reac,i}}$	rate of reaction	$\text{m}^3\ \text{s}^{-1}$
s_{o}	volume of original solid	m^3
s_{r}	volume of reacted solid	m^3
s_{r}^*	critical amount of reacted solid	m^3
t_{CPU}	CPU time	s
t_{f}	simulation stop time	s
U_{col}	particle-particle collision velocity	$\text{m}\ \text{s}^{-1}$
U_{imp}	particle-impeller impact velocity	$\text{m}\ \text{s}^{-1}$
$V_{\text{droplet,mono}}$	volume of droplets	m^3
$\dot{V}_{\text{l}}$	binder flow rate	$\text{m}^3\ \text{s}^{-1}$
V_N	normalisation parameter	m^3
V_{reactor}	reactor volume	m^3
v	total particle volume	m^3
$v_{\text{parent,min}}$	smallest particle that can break	m^3
w	statistical weight	[-]
Y	number of responses	[-]
y^{exp}	responses from experiments	[-]
y^{sim}	responses from simulations	[-]
z	state of the stochastic particle system	[-]

Greek symbols

α_{daughter}	breakage; distribution	[-]
β_{daughter}	breakage; distribution	[-]
Δt	reactor time step	s
ε	particle porosity	[-]
ζ	high-precision solution	[-]
η	binder viscosity	Pa s
η_1	empirical mean of a measured functional	[-]
η_2	empirical variance of a measured functional	[-]
μ_{dsd}	droplet geometric number mean size	m
μ_{psd}	powder geometric number mean size	m
$\nu_{\text{min,max}}$	ratio of the biggest to the smallest possible fragment	[-]
ν_{max}	maximum fraction of the particle that can break	[-]
$\rho_{l_{\text{e}}}$, $\rho_{l_{\text{i}}}$, $\rho_{s_{\text{r}}}$	binder density	$\text{kg}\ \text{m}^{-3}$
$\rho_{s_{\text{o}}}$	material density	$\text{kg}\ \text{m}^{-3}$
σ_{dsd}	droplet geometric number standard deviation	[-]
σ_{psd}	powder geometric number standard deviation	[-]
τ	reactor characteristic residence time	s

Ψ	parameter for breakage	[-]

References

[1] D. Barrasso and R. Ramachandran. Multi-scale modeling of granulation processes: Bi-directional coupling of PBM with DEM via collision frequencies. *Chemical Engineering Research and Design*, 2014. doi:10.1016/j.cherd.2014.04.016.

[2] J. Bouffard, F. Bertrand, and J. Chaouki. A multiscale model for the simulation of granulation in rotor-based equipment. *Chemical Engineering Science*, 81:106 – 117, 2012. doi:10.1016/j.ces.2012.06.025.

[3] A. Braumann, M. J. Goodson, M. Kraft, and P. R. Mort. Modelling and validation of granulation with heterogeneous binder dispersion and chemical reaction. *Chemical Engineering Science*, 62(17):4717 – 4728, 2007. doi:10.1016/j.ces.2007.05.028.

[4] A. Braumann, M. Kraft, and P. R. Mort. Parameter estimation in a multi-dimensional granulation model. *Powder Technology*, 197(3):196 – 210, 2010. doi:10.1016/j.powtec.2009.09.014.

[5] A. Braumann, M. Kraft, and W. Wagner. Numerical study of a stochastic particle algorithm solving a multidimensional population balance model for high shear granulation. *Journal of Computational Physics*, 229(20):7672 – 7691, 2010. doi:10.1016/j.jcp.2010.06.021.

[6] I. Cameron, F. Wang, C. Immanuel, and F. Stepanek. Process systems modelling and applications in granulation: A review. *Chemical Engineering Science*, 60(14):3723 – 3750, 2005. doi:10.1016/j.ces.2005.02.004. Granulation across the length scales - 2nd International Workshop on Granulation.

[7] M. Celnik, R. Patterson, M. Kraft, and W. Wagner. Coupling a stochastic soot population balance to gas-phase chemistry using operator splitting. *Combustion and Flame*, 148(3):158 – 176, 2007. doi:10.1016/j.combustflame.2006.10.007.

[8] A. Chaudhury, H. Wu, M. Khan, and R. Ramachandran. A mechanistic population balance model for granulation processes: Effect of process and formulation parameters. *Chemical Engineering Science*, 107:76 – 92, 2014. doi:10.1016/j.ces.2013.11.031.

[9] A. Darelius, H. Brage, A. Rasmuson, I. N. Björn, and S. Folestad. A volume-based multi-dimensional population balance approach for modelling high shear granulation. *Chemical Engineering Science*, 61(8):2482 – 2493, 2006. doi:10.1016/j.ces.2005.11.016.

[10] C. Denis, M. Hemati, D. Chulia, J.-Y. Lanne, B. Buisson, G. Daste, and F. Elbaz. A model of surface renewal with application to the coating of pharmaceutical tablets in

rotary drums. *Powder Technology*, 130(1-3):174 – 180, 2003. doi:10.1016/S0032-5910(02)00262-0.

[11] B. J. Ennis, G. Tardos, and R. Pfeffer. A microlevel-based characterization of granulation phenomena. *Powder Technology*, 65(1-3):257 – 272, 1991. doi:10.1016/0032-5910(91)80189-P. A Special Volume Devoted to the Second Symposium on Advances in Particulate Technology.

[12] A. Faure, P. York, and R. Rowe. Process control and scale-up of pharmaceutical wet granulation processes: a review. *European Journal of Pharmaceutics and Biopharmaceutics*, 52(3):269 – 277, 2001. doi:10.1016/S0939-6411(01)00184-9.

[13] B. Freireich, J. Li, J. Litster, and C. Wassgren. Incorporating particle flow information from discrete element simulations in population balance models of mixer-coaters. *Chemical Engineering Science*, 66(16):3592 – 3604, 2011. doi:10.1016/j.ces.2011.04.015.

[14] R. Irizarry. Fast compartmental monte carlo simulation of population balance models: Application to nanoparticle formation in nonhomogeneous conditions. *Industrial & Engineering Chemistry Research*, 51(47):15484 – 15496, 2012. doi:10.1021/ie3011116.

[15] S. M. Iveson, J. D. Litster, K. Hapgood, and B. J. Ennis. Nucleation, growth and breakage phenomena in agitated wet granulation processes: a review. *Powder Technology*, 117(1-2):3 – 39, 2001. doi:10.1016/S0032-5910(01)00313-8. Granulation and Coating of Fine Powders.

[16] C. L. M. Jr., P. Rajniak, and T. Matsoukas. Multi-component population balance modeling of granulation with continuous addition of binder. *Powder Technology*, 236:211 – 220, 2013. doi:10.1016/j.powtec.2012.01.027. Special Issue: Pharmaceutical Powders.

[17] C. A. Kastner, G. P. Brownbridge, S. Mosbach, and M. Kraft. Impact of powder characteristics on a particle granulation model. *Chemical Engineering Science*, 97 (0):282 – 295, 2013. doi:10.1016/j.ces.2013.04.032.

[18] J. Li, B. Freireich, C. Wassgren, and J. D. Litster. A general compartment-based population balance model for particle coating and layered granulation. *AIChE Journal*, 58(5):1397 – 1408, 2012. doi:10.1002/aic.12678.

[19] S. Maronga and P. Wnukowski. Modelling of the three-domain fluidized-bed particulate coating process. *Chemical Engineering Science*, 52(17):2915 – 2925, 1997. doi:10.1016/S0009-2509(97)00112-7.

[20] W. J. Menz, S. Shekar, G. P. Brownbridge, S. Mosbach, R. Körmer, W. Peukert, and M. Kraft. Synthesis of silicon nanoparticles with a narrow size distribution: A theoretical study. *Journal of Aerosol Science*, 44(0):46 – 61, 2012. doi:http://dx.doi.org/10.1016/j.jaerosci.2011.10.005.

[21] W. J. Menz, R. I. Patterson, W. Wagner, and M. Kraft. Application of stochastic weighted algorithms to a multidimensional silica particle model. *Journal of Computational Physics*, 248(0):221 – 234, 2013. doi:10.1016/j.jcp.2013.04.010.

[22] W. J. Menz, J. Akroyd, and M. Kraft. Stochastic solution of population balance equations for reactor networks. *Journal of Computational Physics*, 256(0):615 – 629, 2014. doi:10.1016/j.jcp.2013.09.021.

[23] M. Oullion, G. Reynolds, and M. Hounslow. Simulating the early stage of high-shear granulation using a two-dimensional monte-carlo approach. *Chemical Engineering Science*, 64(4):673 – 685, 2009. doi:10.1016/j.ces.2008.08.014. 3rd International Conference on Population Balance Modelling.

[24] R. Patterson, J. Singh, M. Balthasar, M. Kraft, and J. Norris. The linear process deferment algorithm: A new technique for solving population balance equations. *SIAM Journal on Scientific Computing*, 28(1):303–320, 2006. doi:10.1137/040618953.

[25] R. I. Patterson, W. Wagner, and M. Kraft. Stochastic weighted particle methods for population balance equations. *Journal of Computational Physics*, 230(19):7456 – 7472, 2011. doi:10.1016/j.jcp.2011.06.011.

[26] J. M.-H. Poon, C. D. Immanuel, F. J. Doyle, III, and J. D. Litster. A three-dimensional population balance model of granulation with a mechanistic representation of the nucleation and aggregation phenomena. *Chemical Engineering Science*, 63(5):1315 – 1329, 2008. doi:10.1016/j.ces.2007.07.048. Control of Particulate Processes.

[27] G. Reynolds, C. Biggs, A. Salman, and M. Hounslow. Non-uniformity of binder distribution in high-shear granulation. *Powder Technology*, 140(3):203 – 208, 2004. doi:10.1016/j.powtec.2004.01.017. 1st International Workshop on Granulation (Granulation across the length scales: linking microscopic experiments and models to real process operation).

[28] M. Sen and R. Ramachandran. A multi-dimensional population balance model approach to continuous powder mixing processes. *Advanced Powder Technology*, 24 (1):51 – 59, 2013. doi:10.1016/j.apt.2012.02.001.